

The planar pyrochlore antiferromagnet: A large- N analysis

Jean-Sébastien Bernier¹, Chung-Hou Chung¹, Yong Baek Kim¹, and Subir Sachdev²

¹*Department of Physics, University of Toronto, Toronto, Ontario, Canada M5S 1A7*

²*Department of Physics, Yale University, P. O. Box 208120, New Haven, Connecticut 06520-8120*

(Dated: May 22, 2019)

We study possible quantum phases of the Heisenberg antiferromagnet on the planar pyrochlore lattice, also known as the checkerboard lattice or the square lattice with crossings. It is assumed that the exchange coupling on the square-lattice-links is not necessarily the same as those along the crossing links. When all the couplings are the same, this model may be regarded as a two dimensional analog of the pyrochlore antiferromagnet. The large- N limit of the $\text{Sp}(N)$ generalized model is considered and the phase diagram is obtained by analyzing the fluctuation effects about the $N \rightarrow \infty$ limit. We find a topologically-ordered \mathbb{Z}_2 -spin-liquid phase in a narrow region of the phase diagram as well as the plaquette-ordered and staggered spin-Peierls phases as possible quantum-disordered paramagnetic phases.

PACS numbers:

I. INTRODUCTION

Recently frustrated magnets have attracted much interest of theorists and experimentalists as new kinds of frustrated magnetic systems have become available for experimental studies.^{1,2,3} Armed with much progress in understanding the classical frustrated magnets,^{4,5} the attention is now focused on quantum counterparts. Frustration often leads to a large degeneracy of the classical ground states and the resulting frustration-enhanced fluctuations can suppress classical long-range spin order, encouraging the possibility of spin-disordered ground states even in two or three dimensions.^{6,7}

It is not obvious, however, what kinds of quantum ground states may arise as a result of the fluctuations, especially for the small values of spin. Indeed geometrically frustrated magnets seem to allow multifarious quantum-disordered paramagnetic phases, including various translational-symmetry-breaking phases⁸ and the quantum spin liquid phases with fractionalized excitations.^{8,9,10,11} It has been suggested that some of these quantum-disordered phases may also arise in underdoped cuprate superconductors, where the frustration of the spins may occur due to the motion of doped holes.^{12,13}

The possible existence of quantum-disordered phases on the pyrochlore lattice is a particularly interesting question in view of the fact that it is generally harder to suppress a long-range spin order in three dimensions. The progress in understanding this issue has been slower than the cases of two dimensional frustrated magnets mainly due to the significantly bigger Hilbert space.^{14,15,16} To circumvent this difficulty, the planar version of the pyrochlore lattice, also known as the checkerboard lattice or the square lattice with crossings, has been introduced.^{17,18,19,20,21,22,23,24} When all the Heisenberg exchange couplings are the same, the checkerboard lattice has the same local structure of the pyrochlore lattice; a network of corner-sharing tetrahedra. Moreover, the size and topology of the ground state manifold are

also identical in two cases.⁵ Therefore one may expect that the studies of the checkerboard lattice will shed some light on the pyrochlore lattice problem.

In this paper, we examine a Heisenberg model on the checkerboard lattice (illustrated in Fig.1), where the Heisenberg exchange couplings on the horizontal and vertical links are in general different from those along the diagonal links. The motivation for studying such a model partly comes from the fact that no symmetry of the lattice can turn the first neighbor bonds to the second neighbor bonds so that not all the bonds on its tetrahedra are equivalent in contrast to the pyrochlore lattice case. The Hamiltonian for this model can be written as

$$H = J_1 \sum_{\langle ij \rangle} \mathbf{S}_i \cdot \mathbf{S}_j + J_2 \sum_{\text{diagonals}} \mathbf{S}_i \cdot \mathbf{S}_j, \quad (1)$$

where \mathbf{S}_i are $S = 1/2$ operators at the site i . Here $J_1 > 0$ and $J_2 > 0$ are the antiferromagnetic exchange couplings on the nearest-neighbor (horizontal and vertical) links and the second-neighbor (diagonal) links, respectively.

We consider the generalization of the physical spin $\text{SU}(2) \cong \text{Sp}(1)$ symmetry to $\text{Sp}(N)$ and study the quantum ground states of the $\text{Sp}(N)$ Hamiltonian in the large- N limit.⁸ Some of the phases obtained in the large- N limit may not appear in the $\text{SU}(2)$ model. Even these phases, however, may still be relevant to some physical systems whose microscopic Hamiltonians are “near” the parameter space of the original Hamiltonian. For example, these phases may arise when the original system is deformed by substitutional doping or hydrostatic pressure.

More specifically, the first step toward the $\text{Sp}(N)$ generalization starts with the bosonic representation of the $\text{SU}(2)$ spin operators, $\mathbf{S}_i = \frac{1}{2} b_i^\dagger \boldsymbol{\sigma} b_i$, where $\alpha, \beta = \uparrow, \downarrow$ labels two possible spin states of each boson, $b_{i\alpha}$, and the constraint $n_b = b_i^\dagger b_i = 2S$ must be imposed at each site. Then, apart from an additive constant, the

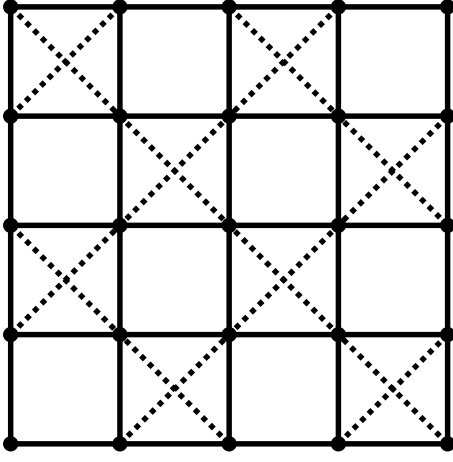


FIG. 1: The checkerboard lattice. The exchange J_1 acts between sites separated by the horizontal or vertical links while the exchange J_2 acts across the diagonal links.

Heisenberg Hamiltonian can be written as

$$H = -\frac{1}{2} \sum_{ij} J_{ij} (\epsilon_{\alpha\beta} b_i^\dagger b_j^\dagger) (\epsilon^{\gamma\delta} b_{i\gamma} b_{j\delta}) \quad (2)$$

where $J_{ij} = J_1$ on the horizontal and vertical links, and $J_{ij} = J_2$ on the diagonal links. Here $\epsilon_{\alpha\beta}$ is the anti-symmetric tensor of $SU(2)$. The generalization to $Sp(N)$ symmetry can be achieved by introducing N flavors of bosons on each site. The constraint must be modified to $n_b = b_i^\dagger b_{i\alpha} = 2NS$, where $\alpha = 1, \dots, 2N$ is a $Sp(N)$ index. For the physical case, $N = 1$, S takes half-integer values. The corresponding $Sp(N)$ Hamiltonian is

$$H = -\frac{1}{2N} \sum_{ij} J_{ij} (\mathcal{J}_{\alpha\beta} b_i^\dagger b_j^\dagger) (\mathcal{J}^{\gamma\delta} b_{i\gamma} b_{j\delta}), \quad (3)$$

where $\mathcal{J}^{\alpha\beta} = \mathcal{J}_{\alpha\beta} = -\mathcal{J}_{\beta\alpha}$ is the generalization of the ϵ tensor of $SU(2)$; it is a $2N \times 2N$ matrix that contains N copies of ϵ along its center block diagonal and vanishes elsewhere.⁸

In the $N \rightarrow \infty$ limit at a fixed boson density per flavor, $n_b/N = 2S = \kappa$, a mean field theory for $S = \kappa/2$ can be obtained and the fluctuations about the mean field state give rise to a gauge theory.⁸ The mean-field phase diagram at $N \rightarrow \infty$ is shown in Fig.3 as a function of $J_2/(J_1 + J_2)$ and $1/S$. At large values of S , various magnetically long-range-ordered (LRO) phases appear and are represented by the ordering wavevector (q_1, q_2) measured in units of $1/(\text{nearest-neighbor spacing})$. The short-range-ordered (SRO) phases at small values of S correspond to the quantum-disordered phases with short-range equal-time spin correlations enhanced at the corresponding wavevectors.

One of the most notable findings in our studies is the existence of a quantum-spin-liquid phase with Z_2 -fractionalized excitations²⁵ in a narrow region of the

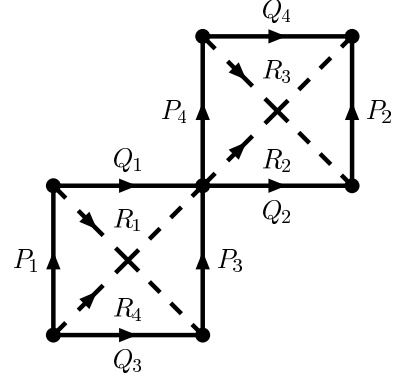


FIG. 2: The four-site unit cell of the checkerboard lattice and the twelve link variables Q_{ij} .

phase diagram (denoted by (π, q) SRO). This region, $J_1 \neq J_2$ and the small values of S , has not been explored in previous works. After taking into account fluctuation effects, the plaquette-ordered state emerges from the (π, π) SRO phase; similarly a staggered spin-Peierls state arises from the $(\pi, 0)$ SRO phase. The result on the (π, π) SRO phase is in accordance with the previous finding of the plaquette-ordered phase for $J_1 = J_2$ and small values of S .^{18,19,20} The transition from the Z_2 quantum-spin-liquid to the plaquette-ordered phase or the staggered spin-Peierls phase is described by a Z_2 gauge theory.^{25,26,27,28} Our results may be also consistent with the large- S study of the $SU(2)$ model with $J_1 \neq J_2$.²⁴ Detailed comparison with the previous works will be made later in this paper.

The rest of this paper is organized as follows. In section II, we describe the mean-field phase diagram and various mean-field phases at $N \rightarrow \infty$. In section III, the effect of singular fluctuations at finite N on the paramagnetic phases is discussed. We explain the relation between the previous works and ours, and conclude in section IV.

II. MEAN FIELD PHASE DIAGRAM

The mean-field theory can be obtained by introducing the directed link fields, $Q_{ij} = -Q_{ji}$. These fields are used to decouple the quartic boson interactions in \mathcal{S} by a Hubbard-Stratonovitch transformation. After this decoupling, the effective action contains the terms

$$\mathcal{S} = \int d\tau \sum_{i>j} \frac{J_{ij}}{2} [N|Q_{ij}|^2 - Q_{ij} \mathcal{J}_{\alpha\beta} b_i^\alpha b_j^\beta + c.c.] + \dots, \quad (4)$$

where τ is the imaginary time and the ellipses represent standard terms which impose the canonical boson commutation relations and the constraint.⁸ At the saddle point of the action, we get

$$\langle Q_{ij} \rangle = \frac{1}{N} \langle \mathcal{J}^{\alpha\beta} b_{i\alpha}^\dagger b_{j\beta}^\dagger \rangle. \quad (5)$$

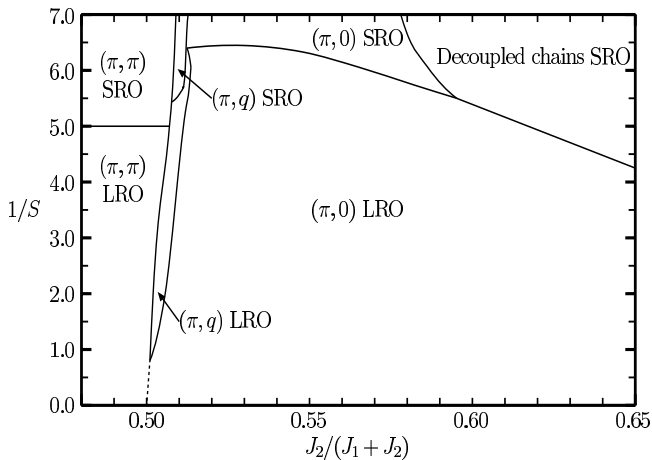


FIG. 3: [Dashed line: first order transition. Solid line: continuous transition.] Large- N phase diagram of the $\text{Sp}(N)$ checkerboard lattice model as a function of $J_2/(J_1 + J_2)$ and $1/S$. The LRO phases break spin-rotation symmetry. The spin order is collinear and commensurate in the (π, π) and $(\pi, 0)$ LRO phases while it is helical and incommensurate in the (π, q) LRO phase. The SRO phases preserve spin-rotation invariance. At $J_1/J_2 = 1$, we find zero expectation value of the diagonal bond variables at all $\kappa = 2S$. The long-range Néel order develops above $\kappa = 2S \approx 0.4$; below this value, the Néel correlations are only short-ranged. In addition, for large values of S , we get the Néel (π, π) LRO for $J_2 < J_1$ and $(\pi, 0)$ LRO for $J_2 > J_1$.

The four-site unit cell of the checkerboard lattice, as depicted in Fig.2, has twelve of these Q_{ij} fields. When S becomes large, the dynamics of \mathcal{S} leads to the condensation of the b_i^α bosons and one obtains a nonzero value of

$$\langle b_i^\alpha \rangle = x_i^\alpha. \quad (6)$$

Since the large- N limit of \mathcal{S} is taken for a fixed value of $\kappa = n_b/N = 2S$, depending on the ratio J_1/J_2 and the value of κ , the ground state of \mathcal{S} at $T = 0$ can either break the global $\text{Sp}(N)$ symmetry and posses magnetic LRO or be $\text{Sp}(N)$ invariant with only SRO; thus the ground state energy should be optimized with respect to variations in $\langle Q_{ij} \rangle$ and x_i^α for different values of J_2/J_1 and κ . We also find that each saddle point may be described by a purely real $\langle Q_{ij} \rangle$. The resulting phase diagram is shown in Fig.3. We describe various magnetically ordered ($x_i^\alpha \neq 0$) and paramagnetic ($x_i^\alpha = 0$) phases as follows.

A. Magnetically ordered phases

1. Néel (π, π) LRO state

This is the long-range-ordered state in which $\langle \mathbf{S}_i \rangle$ is collinearly polarized in opposite directions on two sublattices. In the appropriate gauge, the expectation values

of link variables are nonzero and equal on the horizontal (Q) and vertical (P) links, while the values on the diagonal links (R) are zero.

2. $(\pi, 0)$ and $(0, \pi)$ LRO states

This magnetically ordered phase is characterized by nonzero values of $\langle Q_{ij} \rangle$ on the horizontal and diagonal links for the $(\pi, 0)$ LRO state or on the vertical and diagonal links for the $(0, \pi)$ LRO state. There are two gauge-nonequivalent choices for the values of R_1, R_2, R_3 and R_4 . One state has $R_1 = R_2 = R_3 = R_4$ with $P = 0$ and $Q \neq 0$, and the other has $R_1 = R_3 = -R$ and $R_2 = R_4 = R$ with $P \neq 0$ and $Q = 0$. These two states are interchanged under a $\pi/2$ rotation. Moreover, these states can be understood as diagonally coupled horizontal or vertical Heisenberg antiferromagnetic chains.

3. Helical (π, q) and (q, π) LRO states

This helically-ordered phase is characterized by nonzero values of $\langle Q_{ij} \rangle$ on the horizontal, vertical and diagonal links. Once again, our results indicate that there are two gauge-nonequivalent choices for the values of R_1, R_2, R_3 and R_4 . One state has $R_1 = R_2 = R_3 = R_4$ with $Q > P$ and the other has $R_1 = R_3 = -R$ and $R_2 = R_4 = R$ with $P > Q$. These two states are interchanged under a $\pi/2$ rotation and correspond to spirals ordered in the horizontal or vertical directions. Notice that this is a long-range incommensurate spin order and the spin structure factor peaks at the incommensurate wavevector (π, q) or (q, π) . Here q varies continuously as J_2/J_1 changes.

B. Paramagnetic phases

1. Decoupled chains

As its name suggests, this phase is a grid of decoupled Heisenberg antiferromagnetic chains. In the large- N limit, it corresponds to the solution where the $\langle Q_{ij} \rangle$ are nonzero only on the diagonal links.

2. (π, π) SRO state

This state is obtained by quantum disordering the Néel state (it occurs at $\kappa < 0.4$). The expectation values of Q_{ij} have the same structure as those of the Néel state. As described in previous works, the quantum fluctuations in this phase can be understood via a compact $U(1)$ gauge theory.⁸ This theory is always confining, thus the b_i^α bosons bind to form a $S = 1$ quasiparticle above a spin

gap.⁸ At finite N , gauge-theoretic consideration of singular fluctuations lead to the plaquette order (see section III).

3. $(\pi, 0)$ and $(0, \pi)$ SRO state

This is the quantum-disordered state of the $(\pi, 0)$ or $(0, \pi)$ LRO state and the expectation values of Q_{ij} have a similar structure as those of its ordered counterpart. Even though this state has a gap to all spin excitations, the symmetry of $\pi/2$ rotations between the vertical and horizontal directions is broken. Again, the gauge-theoretic consideration at finite N leads to the staggered spin-Peierls phase (see section III).

4. (π, q) and (q, π) SRO state

This state is obtained by quantum disordering the (π, q) or (q, π) LRO state and the expectation values of Q_{ij} have a similar structure as those of its ordered counterpart. As discussed in previous works, nonzero expectation values of the diagonal link fields leads to the presence of the “charge”-2 Higgs scalar coupled to a compact U(1) gauge field.^{8,10} As a result, this phase corresponds to the deconfined phase of the Z_2 gauge theory and supports deconfined spinons with $S = 1/2$ above the spin gap.^{25,26,27,28} Again, even though this state has a gap to all spin excitations, the symmetry of $\pi/2$ rotations between the vertical and horizontal directions is broken. This phase is topologically ordered and it leads to an additional fourfold degeneracy of the ground state on a torus.^{25,26,27,28}

III. FLUCTUATION EFFECT AND EMERGENCE OF TRANSLATIONAL-SYMMETRY-BREAKING PHASES

In this section, we will discuss the influence of the fluctuations about the mean-field on the spin-singlet sector of the (π, π) and $(\pi, 0)$ SRO phases. It has been known that the fluctuations at finite- N can be understood via the compact U(1) gauge theory.⁸ Regular perturbative corrections in $1/N$ and higher-orders do not qualitatively change the mean-field ground states at $N \rightarrow \infty$. On the other hand, singular effects of the hedgehog instantons in the gauge theory and their Berry phases lead to the qualitative changes, typically the emergence of various translational-symmetry-breaking phases⁸. For simplicity, we will only consider the case where $2SN$ is an odd integer. Notice that, for the physical SU(2) case with $N = 1$, it corresponds to the half-integer values of S .

In the dual formulation, these instanton effects take the form of a statistical mechanical “interface” or “height” model. In most cases this height model has a limiting

regime where it can be mapped onto a quantum dimer model, and this yields an appealing physical interpretation of the computation. However, the mapping to the dimer model is *not available in all cases*, and here the instanton analysis is a bit more subtle. It turns out that the $(\pi, 0)$ SRO phase is one of the cases where the dimer model mapping is absent. Consequently, we will eschew the dimer interpretation here, and present details of the computation using the compact U(1) gauge theory.

As has been argued elsewhere^{8,29} spin fluctuations in the paramagnetic phase of collinear antiferromagnets are described by the following compact U(1) lattice gauge theory

$$\mathcal{Z}_A = \prod_{j\mu} \int_0^{2\pi} \frac{dA_{j\mu}}{2\pi} \exp \left(\sum_{\square} \frac{1}{K_a} \cos(\epsilon_{\mu\nu\lambda} \Delta_\nu A_{j\lambda}) - i \sum_j \eta_j A_{j\tau} \right), \quad (7)$$

Here j denotes the sites of cubic lattice in discretized spacetime, the subscript a the sites of the dual cubic lattice, μ, ν, λ extend over x, y, τ , Δ_μ is the discrete lattice derivative in the μ direction, $A_{j\mu}$ is the compact U(1) gauge field, and the coupling K_a can take distinct values of different dual lattice sites as determined by the symmetry of the underlying lattice. The fixed field η_j is the key quantity which distinguishes different SRO phases, and encapsulates the staggering of the spins in the local collinear order. It has the values

$$\eta_j = \begin{cases} (-1)^{j_x + j_y} & \text{for } (\pi, \pi) \text{ SRO} \\ (-1)^{j_x} & \text{for } (\pi, 0) \text{ SRO} \end{cases} \quad (8)$$

Note that η_j is independent of the τ co-ordinate.

We now proceed with a duality mapping of (7). For the (π, π) SRO phase, the procedure is essentially identical to that in Ref. 29, and it leads to a dual interface model identical to that found for the (π, π) SRO phase of the Shastry-Sutherland lattice¹⁰. From these results we obtain the plaquette-ordered state as shown in Fig. 4(a). Similar conclusions were also reached in Ref 19.

We now apply the same procedure to the $(\pi, 0)$ SRO phase. The only difference here is in the value of η_j in (8), but otherwise the initial steps are the same as before²⁹. First, we find an integer valued vector field, $a_{a\mu}^0$ on the links of the dual lattice such that its curl is a vector η_j pointing in the τ direction

$$\epsilon_{\mu\nu\lambda} \Delta_\nu a_{a\mu}^0 = \eta_j \delta_{a\tau}. \quad (9)$$

A convenient choice for $a_{a\mu}^0$ is shown in Fig. 5. Then, we write the cosine term in \mathcal{Z}_A in the Villain periodic Gaussian form, and perform a standard duality transformation by the Poisson summation method. This maps \mathcal{Z}_A to a dual interface model

$$\mathcal{Z}_h = \sum_{\{h_a\}} \exp \left(- \sum_{a,\mu} \frac{K_a}{2} (\Delta_\mu h_a + a_{a\mu}^0)^2 \right). \quad (10)$$

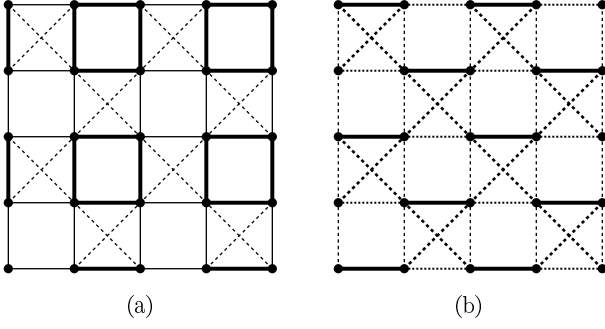


FIG. 4: Singular fluctuations at finite N lead to (a) the plaquette-ordered phase in the (π, π) SRO state and (b) the staggered spin-Peierls phase in the $(\pi, 0)$ SRO state.

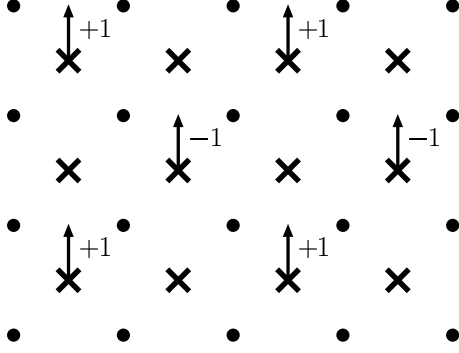


FIG. 5: Specification of the non-zero values of the fixed field $a_{a\mu}^0$. The circles are the sites of the direct lattice, j , while the crosses are the sites of the dual lattice, a ; the latter are also offset by half a lattice spacing in the direction out of the paper (the $\mu = \tau$ direction). The $a_{a\mu}^0$ are all zero for $\mu = \tau, x$, while the only non-zero values of $a_{a\mu}^0$ are shown above.

Here h_a are the integer valued heights of the interface model. Next, we decompose $a_{a\mu}^0$ into its curl and divergence free parts by writing

$$a_{a\mu}^0 = \Delta_\mu \zeta_a + \epsilon_{\mu\nu\lambda} \Delta_\nu \mathcal{Y}_{j\lambda}. \quad (11)$$

The values of the new fields ζ_a and \mathcal{Y}_j are shown in Fig. 6 and Fig. 7. The values of ζ_a will be particularly important to us, and these take the values $\zeta_W = 1/4, \zeta_X = 1/4, \zeta_Y = 3/4, \zeta_Z = 3/4$ on the four dual sublattices W, X, Y, Z shown in Fig. 6. Inserting (11) into (10) we obtain the final form of the interface model

$$\mathcal{Z}_h = \sum_{\{H_a\}} \exp \left(- \sum_a \frac{e_a^2}{2} (\Delta_\mu H_a)^2 \right), \quad (12)$$

where

$$H_a \equiv h_a + \zeta_a. \quad (13)$$

Finally, as is usual in the mappings from interface models to sine-Gordon models, we can ‘soften’ the integer value constraint on the h_a , and replace H_a by a real valued field χ_a which experiences a cosine potential with minima at

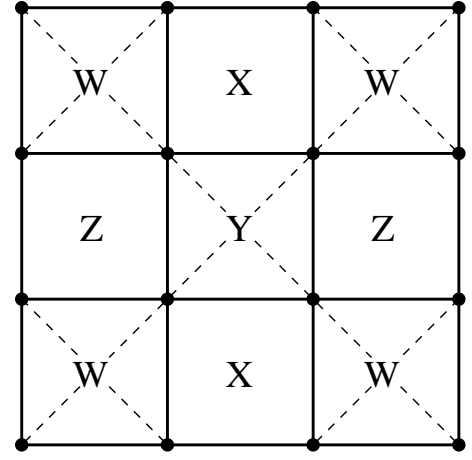


FIG. 6: The four dual sublattices upon which the height offsets take the values $\zeta_W = 1/4, \zeta_X = 1/4, \zeta_Y = 3/4$, and $\zeta_Z = 3/4$.

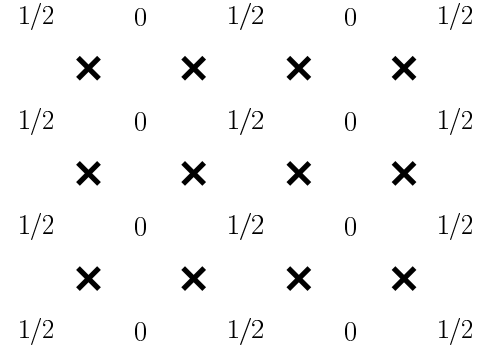


FIG. 7: Specification of the non-zero values of the fixed field $\mathcal{Y}_{j\mu}$. Only the $\mu = \tau$ components are non-zero, and these are shown above.

positions satisfying (13). This yields finally a sine Gordon model for the field $\chi_a(\tau)$ with the action

$$\begin{aligned} \mathcal{S}_\chi = & \int d\tau \left[\frac{K}{2} \sum_{\langle ab \rangle} (\chi_a - \chi_b)^2 \right. \\ & \left. + \sum_a \left\{ \frac{K_\tau}{2} (\partial_\tau \chi_a)^2 - y_a \cos(2\pi(\chi_a - \zeta_a)) \right\} \right] \quad (14) \end{aligned}$$

where the sum over $\langle ab \rangle$ extends over nearest neighbor sites, and K is the stiffness towards spatial fluctuations of the interface height. K_τ is the corresponding stiffness towards time-dependent fluctuations, and, for simplicity, its value is assumed to be independent of a . The symmetry of the lattice requires that the strength of the periodic potential take two possible values, $y_a = y_1$ or $y_a = y_2$ depending upon whether the plaquette a has diagonal J_2 links across it or not.

The optimal interface configurations can be determined by the minimization of \mathcal{S}_χ by a set of time-independent values of χ_W, χ_X, χ_Y , and χ_Z . Then, the

problem reduces to the minimization of the following energy as a function of four real variables:

$$E_\chi = K \left[(\chi_X - \chi_W)^2 + (\chi_W - \chi_Y)^2 + (\chi_Y - \chi_Z)^2 + (\chi_Z - \chi_X)^2 \right] - y_1 \left[\sin(2\pi\chi_W) - \sin(2\pi\chi_Y) \right] - y_2 \left[\sin(2\pi\chi_X) - \sin(2\pi\chi_Z) \right] \quad (15)$$

Our analysis here is valid only for small y_1 and y_2 , so we will analytically determine the minima in power series in $y_{1,2}$. Let us define

$$\begin{aligned} \chi_W &= \chi_1 + \chi_2 + \chi_3 \\ \chi_X &= \chi_1 - \chi_2 + \chi_4 \\ \chi_Y &= \chi_1 + \chi_2 - \chi_3 \\ \chi_Z &= \chi_1 - \chi_2 - \chi_4. \end{aligned} \quad (16)$$

At the saddle points of E_χ , we obtain

$$\begin{aligned} \chi_2 &= \frac{\pi^3(y_2^2 - y_1^2)}{16K^2} \sin(4\pi\chi_1) + \mathcal{O}(y_{1,2}^4) \\ \chi_3 &= \frac{\pi y_1}{2K} \cos(2\pi\chi_1) + \mathcal{O}(y_{1,2}^3) \\ \chi_4 &= \frac{\pi y_2}{2K} \cos(2\pi\chi_1) + \mathcal{O}(y_{1,2}^3). \end{aligned} \quad (17)$$

The average interface height, χ_1 , is determined by the minimization of

$$E_\chi = E_0 + A \cos(4\pi\chi_1) + B \cos(8\pi\chi_1) + \dots, \quad (18)$$

where E_0 is a constant independent of χ_1 ,

$$\begin{aligned} A &= -\frac{\pi^2}{2K}(y_1^2 + y_2^2) + \frac{\pi^6}{3K^3}(y_1^4 + y_2^4) \\ B &= \frac{11\pi^6}{96K^3}(y_1^4 + y_2^4) - \frac{\pi}{16K^3}(y_1^2 y_2^2), \end{aligned} \quad (19)$$

and all omitted terms are of order $y_{1,2}^6$ or higher. We now have to minimize (18) to determine χ_1 . Then from (17), we know $\chi_{2,3,4}$, and hence the configuration of the interface heights. For small y_1 and y_2 , $A < 0$ and $|A| \gg |B|$, therefore the saddle point solution is given by $\chi_1 = 0, 1/2$. Taking $\chi_1 = 0$, we get $\chi_2 = 0$, $\chi_3 = \frac{\pi y_1}{2K}$ and $\chi_4 = \frac{\pi y_2}{2K}$. Subsequently, using (16), we obtain

$$\chi_W = \frac{\pi y_1}{2K}, \chi_X = \frac{\pi y_2}{2K}, \chi_Y = -\frac{\pi y_1}{2K}, \chi_Z = -\frac{\pi y_2}{2K} \quad (20)$$

Following the previous work by Read and Sachdev,⁸ the static “electric field” in the compact U(1) gauge theory on the links of the lattice of spins is given by $iE_\alpha = g \sum_\beta \epsilon_{\alpha\beta} \Delta_\beta \chi$, where $\alpha, \beta = x, y$. From this equation, we find $iE_x = \pm g\pi(y_2 + y_1)/(2K)$ depending on whether the electric field resides in the even (+) or odd (−) row, and $iE_y = \pm g\pi(y_2 - y_1)/(2K)$ depending on whether the electric field resides in an odd (+)

or even (−) column. Finally, these electric fields can be related to the underlying spin correlation function: this requires determining the analog of the couplings in (3.17) of Ref.30. However, the main effect can also be deduced here from simple symmetry considerations. The values of η_j in (8) show that we can define an orientation to every horizontal link of the square lattice (from $\eta_j = +1$ to $\eta_j = -1$) but not to the vertical links. Consequently, the uniform horizontal electric field strengthens every link oriented parallel to it (say) and weakens those antiparallel to. Also, there is no corresponding modulation in the vertical direction. Taken together, these considerations show that the static electric fields determined above lead to the staggered dimerization pattern shown in Fig.4 (b).

IV. CONCLUSION AND RELATION TO PREVIOUS WORKS

We investigated quantum ground states of the $\text{Sp}(N)$ antiferromagnetic Heisenberg model on the checkerboard lattice, where the Heisenberg exchange couplings on the horizontal and vertical links (J_1) are in general not the same as those along the diagonal links (J_2). The mean-field phase diagram of the model was obtained in the $N \rightarrow \infty$ limit as a function of $J_2/(J_1 + J_2)$ and $1/S$. We found various magnetically-ordered phases at large values of S , and the corresponding quantum-disordered paramagnetic phases at small values of S . The effect of singular fluctuations about the mean-field states was examined in the quantum-disordered paramagnetic phases and it leads to the emergence of various translational-symmetry breaking phases.

At small values of S , when J_2 is small or comparable to J_1 , the ground state is the plaquette-ordered phase (shown in Fig.4 (a)) that is obtained by quantum-disordering the Néel ordered state; this is as predicted in a related study on a lattice with a similar symmetry¹⁰, and agrees with the studies of the $J_1 = J_2$ case by the exact diagonalization and large- N studies.^{18,19,20} As J_2 is increased, a topologically ordered Z_2 -spin-liquid phase²⁵ appears in a narrow region of the phase diagram. This phase is the quantum-disordered phase of the (π, q) LRO phase. If J_2 is further increased, the ground state becomes the staggered spin-Peierls phase (shown in Fig.4 (b)) that is obtained by quantum-disordering the $(\pi, 0)$ LRO phase. The transition from the plaquette-ordered (or the staggered spin-Peierls) phase to the Z_2 -spin-liquid phase should be described by a Z_2 gauge theory.^{8,10,19,25,26,27,28} On the other hand, in the $J_2 \gg J_1$ limit, the mean-field ground state is the decoupled-chains SRO phase. At finite N , a weak coupling between the decoupled chains will be generated and this may lead to the “sliding-Luttinger-liquid” phase previously discovered in the study of the $J_1 \neq J_2$ case with $S = 1/2$; Our large- N study cannot capture this physics.

When S is very large, there exist two magnetically ordered phases; (π, π) LRO for $J_2 < J_1$ and $(\pi, 0)$ LRO for

$J_2 > J_1$. This result is consistent with the recent large- S study of the $J_1 \neq J_2$ case.²⁴ At intermediate values of S , however, there exists an additional magnetically ordered phase, the (π, q) LRO phase, between the (π, π) and $(\pi, 0)$ LRO phases. This incommensurate ordered phase is the parent state of the Z_2 -spin-liquid phase.

Finally, it is intriguing to see the emergence of the spin-liquid-phase in the planar pyrochlore (albeit in a narrow region of the phase diagram) in view of the fact that the existence of a three dimensional spin-liquid-phase was

recently proposed in the easy-axis limit of the antiferromagnetic Heisenberg model on the three dimensional pyrochlore lattice.³¹

Acknowledgment: We thank Aspen Center for Physics where a part of this work was carried out, for its hospitality. This work was supported by the NSERC of Canada, Canadian Institute for Advanced Research, Canada Research Chair Program, Sloan Fellowship (JSB, CHC, YBK), and the US NSF grant DMR-0098226 (SS).

-
- ¹ For an experimental review, see P. Schiffer and A. P. Ramirez, *Comments Condens. Matter Phys.* **18**, 21 (1996).
 - ² H. Kakeyama *et al*, *Phys. Rev. Lett.* **82**, 3168 (1999); H. Kakeyama *et al*, *Phys. Rev. Lett.* **84**, 5876 (2000).
 - ³ R. Coldea, D. A. Tennant, A. M. Tsvelik, and Z. Tylczynski, *Phys. Rev. Lett.* **86**, 1335 (2001); R. Coldea, D. A. Tennant, and Z. Tylczynski, *cond-mat/0307025*.
 - ⁴ See, for example, R. Moessner, *cond-mat/0010301*.
 - ⁵ R. Moessner and J. T. Chalker, *Phys. Rev. Lett.* **80**, 2929 (1998); *Phys. Rev. B* **58**, 12049 (1998).
 - ⁶ J. Villain, *Z. Phys. B* **33**, 31 (2001).
 - ⁷ A. B. Harris, A. J. Berlinsky, and C. Bruder, *J. Appl. Phys.* **69**, 5200 (1991).
 - ⁸ S. Sachdev, *Phys. Rev. B* **45**, 12377 (1992); N. Read and S. Sachdev, *Phys. Rev. Lett.* **66**, 1773 (1991); S. Sachdev and N. Read, *Int. J. Mod. Phys. B* **5**, 219 (1991).
 - ⁹ C. H. Chung, J. B. Marston, and R. H. McKenzie, *J. Phys: Condens. Matter* **13**, 5159 (2001).
 - ¹⁰ C. H. Chung, J. B. Marston, and S. Sachdev, *Phys. Rev. B* **64**, 134407 (2001).
 - ¹¹ C. H. Chung, K. Voelker, and Y. B. Kim, *Phys. Rev. B* **68**, 094412 (2003).
 - ¹² M. Vojta, Y. Zhang, and S. Sachdev, *Phys. Rev. B* **62**, 6721 (2000).
 - ¹³ P. W. Anderson, *Science* **235**, 1196 (1987).
 - ¹⁴ A. Koga and N. Kawakami, *Phys. Rev. Lett.* **84**, 1808 (2000).
 - ¹⁵ B. Canals and C. Lacroix, *Phys. Rev. Lett.* **80** 2933 (1998); *Phys. Rev. B* **61** 1149 (2000).
 - ¹⁶ H. Tsunetsugu, *J. Phys. Soc. Japan*, **70** 640 (2001); *Phys. Rev. B* **65**, 024415 (2002).
 - ¹⁷ E. H. Lieb and P. Schupp, *Phys. Rev. Lett.* **83**, 5362 (1999).
 - ¹⁸ S. E. Palmer and J. T. Chalker, *Phys. Rev. B* **64**, 094412 (2001).
 - ¹⁹ R. Moessner, O. Tchernyshyov, and S. L. Sondhi, *cond-mat/0106286*.
 - ²⁰ J.-B. Fouet, M. Mambrini, P. Sindzingre, and C. Lhuillier, *Phys. Rev. B* **67**, 054411 (2003).
 - ²¹ O. A. Starykh, R. R. P. Singh, and G. C. Levin, *Phys. Rev. Lett.* **88**, 167203 (2002).
 - ²² P. Sindzingre, J.-B. Fouet, and C. Lhuillier, *Phys. Rev. B* **66**, 174424 (2002).
 - ²³ E. Berg, E. Altman, and A. Auerbach, *Phys. Rev. Lett.* **90**, 147204 (2003).
 - ²⁴ O. Tchernyshyov, O. A. Starykh, R. Moessner, and A. G. Abanov, *cond-mat/0301303*.
 - ²⁵ D. S. Rokhsar and S. A. Kivelson, *Phys. Rev. Lett.* **61**, 2376 (1988); S. A. Kivelson, *Phys. Rev. B* **39**, 259 (1989); N. Read and B. Chakraborty, *Phys. Rev. B* **40**, 7133 (1989); R. A. Jalabert and S. Sachdev, *Phys. Rev. B* **44**, 686 (1991); X.-G. Wen, *Phys. Rev. B* **44**, 2664 (1991); T. Senthil and M. P. A. Fisher, *Phys. Rev. B* **63**, 134521 (2001); R. Moessner, S. L. Sondhi, and E. Fradkin, *Phys. Rev. B* **65**, 024504 (2002).
 - ²⁶ L. Balents, M. P. A. Fisher, and S. M. Girvin, *Phys. Rev. B* **65**, 224412 (2002).
 - ²⁷ C. Nayak and K. Shtengel, *Phys. Rev. B* **64**, 064422 (2001).
 - ²⁸ E. Demler, C. Nayak, H.-Y. Kee, Y. B. Kim, T. Senthil, *Phys. Rev. B* **65**, 155103 (2002).
 - ²⁹ S. Sachdev, *Proceedings of the International Conference on Theoretical Physics*, Paris, *Annales Henri Poincare* **4**, 559 (2003), *cond-mat/0304137*.
 - ³⁰ N. Read and S. Sachdev, *Phys. Rev. B* **42**, 4568 (1990).
 - ³¹ Michael Hermele, Matthew P. A. Fisher, and Leon Balents, *cond-mat/0305401*